

Effect of enzymatic degradation of chitosan in polyhydroxybutyrate/chitosan/calcium phosphate composites on in vitro osteoblast response

Maria Giretova¹ · Lubomir Medvecký¹ · Radoslava Stulajterova¹ · Tibor Sopcak¹ · Jaroslav Briancin² · Monika Tatarkova¹

Received: 9 May 2016 / Accepted: 14 October 2016 / Published online: 21 October 2016
© Springer Science+Business Media New York 2016

Abstract Polyhydroxybutyrate/chitosan/calcium phosphate composites are interesting biomaterials for utilization in regenerative medicine and they may be applied in reconstruction of deeper subchondral defects. Insufficient informations were found in recent papers about the influence of lysozyme degradation of chitosan in calcium phosphate/chitosan based composites on in vitro cytotoxicity and proliferation activity of osteoblasts. The effect of enzymatic chitosan degradation on osteoblasts proliferation was studied on composite films in which the porosity of origin 3D scaffolds was eliminated and the surface texture was modified. The significantly enhanced proliferation activity with faster population growth of osteoblasts were found on enzymatically degraded biopolymer composite films with α -tricalcium phosphate and nanohydroxyapatite. No cytotoxicity of composite films prepared from lysozyme degraded scaffolds containing a large fraction of low molecular weight chitosans (LMWC), was revealed after 10 days of cultivation. Contrary to above in the higher cytotoxicity origin untreated nanohydroxyapatite films and porous composite scaffolds. The results showed that the synergistic effect of surface distribution, morphology of nanohydroxyapatite particles, microtopography and the presence of LMWC due to chitosan degradation in composite films were responsible for compensation of the

cytotoxicity of nanohydroxyapatite composite films or porous composite scaffolds.

1 Introduction

Composites with biopolymer matrix and calcium phosphate bioactive component represent systems, which are currently interesting for utilization in reconstruction and regenerative medicine, maxillofacial surgery and other medicine fields. The chitosan belongs to hydrophilic biopolymer polysaccharide types with inductive and stimulation activity on connective tissue rebuilding [1]. Because of the sufficient swelling and water uptake of chitosan based composites during the preparation, it make possible to create large-porous substrates after lyophilization. A low addition of nanohydroxyapatite (up to 2 wt%) to the chitosan solution with following formation of highly porous scaffolds by lyophilization showed an enhanced proliferation activity and population growth of osteoblasts but no effect of different molecular weight of chitosan on proliferation was found [2]. The nanohydroxyapatite or nano- β -tricalcium phosphate addition to chitosan improved the bioactivity of composite scaffolds and affected the apatite formation on surface [3, 4]. Chitosan scaffolds with higher deacetylation degree (DD) more supported the attachment and proliferation of L929 cells than more acetylated ones [5]. The influence of chitosan addition in the form of hardening liquid to calcium phosphate cement (CPC) mixture on viability and growth rate of osteoblasts was evaluated by Hesareki and Nezafati [6]. It was demonstrated improving of CPC flexural strength without affecting osteoblast viability on CPC/chitosan micro- or macro-porous composites [7]. The comparable cell viability on chitosan/nanohydroxyapatite and chitosan/

✉ Maria Giretova
mgiretova@saske.sk

¹ Institute of Materials Research of SAS, Watsonova 47, 04001 Kosice, Slovakia

² Institute of Geotechnics of SAS, Watsonova 47, 04001 Kosice, Slovakia

microhydroxyapatite macroporous scaffolds with hydroxyapatites from marine fish bone was shown without observable cytotoxicity [8]. The low molecular weight chitosan in CPC composites exhibited both the strong antibactericidal activity and the severe cytotoxicity [9]. On the other hand, no effect of the chitosan molecular weight (depolymerized with nitric acid) on antibacterial action was observed but chitosans with a low DD had enhanced antibacterial activity [10]. Treatment of MC3T3-E1 cells in solutions with the water soluble low molecular chitosan (amylase hydrolysis) caused a significant increase in osteoblastic activity [11]. Above results verified the strong influence of the molecular weight of chitosan on activity of cells and bacteria. The poly(3-hydroxybutyrate) (PHB) represents natural biodegradable and hydrophobic biopolymer utilized in blends and composites. The porous hydroxyapatite reinforced polyhydroxybutyrate-co-valerate scaffolds (2 wt% hydroxyapatite) showed the rise in stiffness, strength, and improving in-vitro bioactivity of scaffolds due to presence of the bioactive hydroxyapatite component [12]. A porous biphasic calcium phosphate/chitosan/polyhydroxybutyrate asymmetric membrane stimulated proliferation of gingival fibroblasts and osteoblasts [13]. Polyhydroxybutyrate/hydroxyapatite nanocomposite exhibited a pronounced cell differentiation resulting from a high surface roughness and large amount of exposed hydroxyapatite [14]. The addition of a nano-sized reinforcing phase to PHBV (polyhydroxybutyrate-co-valerate) reduced the proinflammatory response and osteoclasts failed to form of the functional actin rings or resorption pits on composite materials [15]. It has been shown that the degradation of biopolymer component in PHBV/HA and PHBV/TCP composites increased more rapidly and the mineralized reactions occurred on PHBV/TCP in SBF solution [16]. The miscibility and mutual intermolecular interaction were demonstrated between polyhydroxybutyrate and chitosan chains [17, 18]. The nanofibrous PHBV–chit scaffolds had good fibroblast proliferation activity and a superior ability for improving fibroblast adhesion [19]. Similarly, the organic soluble (in chloroform) PHB–chit composites exhibited non-cytotoxic behavior [20]. A significant reduction in the average molecular weight of biopolymers was found in pure chitosan scaffold after precipitation of the chitosan in the presence of propylene carbonate and in blends after mutual mixing with PHB [23]. No or limited informations were found in recent papers about the influence of lysozyme degradation of chitosan in calcium phosphate/chitosan or calcium phosphate/chitosan/PHB composites on in vitro cytotoxicity and proliferation activity of osteoblasts despite of that lysozyme represents enzyme normally present in human body fluids like e.g. serum and it can affect the properties of chitosan composites after implantation of into body.

In this paper, the influence of microstructure, physico-chemical properties and enzymatic degradation of polyhydroxybutyrate/chitosan/calcium phosphate composites on in vitro osteoblast response were studied. The stable nanohydroxyapatite and transformable α -tricalcium phosphate (TCP) particles or powder tetracalcium phosphate/nanomonetite cement composite mixtures (TTCPMH) were used as fillers in biopolymer polyhydroxybutyrate/chitosan system. The in vitro osteoblast response on composites was evaluated on untreated highly porous scaffolds with large-scale pores and the effect of chitosan degradation was studied on compact composite films with eliminated pores after pressing the origin porous scaffolds.

2 Experimental procedure

2.1 Synthesis of calcium phosphates

Calcium-deficient nanohydroxyapatite (HAP) was synthesized by the coprecipitation of $\text{Ca}(\text{NO}_3)_2 \cdot 4\text{H}_2\text{O}$ (Sigma-Aldrich, analytical grade, concentration of 0.5 mol dm^{-3}) and $(\text{NH}_4)_2\text{HPO}_4$ (Sigma-Aldrich, analytical grade, concentration of 0.5 mol dm^{-3}) solutions with a molar ratio of $\text{Ca/P} = 1.66$. The pH was kept at 10.5 by adding of $\text{NH}_3(\text{aq})$ (1:1). Ageing time was 72 h. Precipitates were washed with distilled water and filtered over the membrane filter (Millipore, $0.2 \mu\text{m}$ pore size). Nanohydroxyapatite (HAP) powders were dried at 110°C for 2 h.

Tetracalcium phosphate ($\text{Ca}_4(\text{PO}_4)_2\text{O}$) was prepared by annealing an equimolar mixture of calcium carbonate (CaCO_3 , analytical grade, SigmaAldrich) and dicalcium phosphate anhydrous (DCPA) (CaHPO_4 , Fluka, (Ph. Eur.), Fluka), at 1450°C for 5 h. After cooling, the product was crushed by milling in a planetary ball mill (Fritsch) for 2 h and the phase purity was evaluated using the X-ray powder diffraction analysis (XRD, Philips X Pert Pro). The powder tetracalcium phosphate/nanomonetite cement mixture (TTCPMH) was synthesized by in situ reaction between tetracalcium phosphate and diluted solution of the orthophosphoric acid (analytical grade, Merck) in ethanol (1:4). The ethanolic orthophosphoric acid solution/tetracalcium phosphate ratio was 1. The H_3PO_4 was added at such an amount that the final Ca/P mole ratio in powder mixture was equal to 1.67, which corresponds to the Ca/P mole ratio in HA.

α -TCP was synthesized by solid state reaction of calcium carbonate (CaCO_3 , analytical grade, SigmaAldrich) and dicalcium phosphate anhydrous (DCPA) (CaHPO_4 , Fluka, (Ph. Eur.) powder mixture at 1350°C for 2 h and following crushing in agate mortar. The Ca/P ratio was 1.5 and starting powder reactants were homogenized in ball mill (agate balls) in distilled water.

2.2 Preparation of blends and composites

The blends with polyhydroxybutyrate (GoodFellow)/chitosan (SigmaAldrich, middle) ratio equals 1:1, were prepared by mixing of PHB (dissolved in propylene carbonate) and chitosan (in 1 % acetic acid) solutions. The composites with 50 wt% of calcium phosphate component were prepared by the mutual mixing of calcium phosphate, PHB (propylene carbonate was used as solvent), and chitosan solutions (1 % acetic acid solution as solvent) in corresponding amounts. Note that the same solution volumes were used for preparation of composites. Mixing was carried out using a magnetic stirrer at 400 rpm. Final suspensions were filtered, washed with acetone and molded into block form (4 mm × 25 mm × 3 mm), cut to smaller parts (4 × 4 × 3 mm), freeze-dried at -20 °C and lyophilized (Ilshin) for 6 h. Samples in the form of thin film were prepared by pressing of porous scaffolds at 90 MPa in mold with 6 mm diameter and 200 nm thickness.

2.3 Characterization methods

The chemical interactions were evaluated by FTIR spectroscopy (Shimadzu, IRAffinity1, KBR method). The microstructure of scaffolds was observed by field emission scanning electron microscopy (JEOL FE SEM JSM-7000F) after coating with gold (ion sputter, FINE COAT, Jeol JFC -1100; 1.2 kV, 4 mA for 10 min). The distribution of molecular weights of chitosan in origin blends and blends after 3 days of chitosan degradation in lysozyme, was determined by gel permeation chromatography (GPC, Watrex, RI detector). The separation was carried out on the PL gel mixed OH 8 μm at 1 mL/min flow rate of mobile phase (phosphate buffered saline, PBS, pH = 6). The calibrations of molecular weights in blends were carried out using dextrans with various average molecular weights. The molecular weight distribution of chitosan in samples was evaluated by Clarity software. The chitosan degradation in scaffolds by lysozyme solution (2 mg/mL, PBS, pH = 7.4) at 37 °C was characterized by the amount of reducing sugars created during enzymolysis at selected times. The reducing ends of sugars (RES) were determined by the potassium ferricyanide method described by Ni et al. [21]. N-Glucosamine (Sigma-Aldrich) solutions were used as standards, and determination was carried out at 65 °C by the kinetic measurement of absorbance at 420 nm after 10 min (UV-1800, Shimadzu) from reagent addition and sample mixing. The contents of RES in samples were calculated as an amount of N-Glucosamine related to sample mass. The surface roughness of the samples was measured by the 3D optical profilometer (PLu Neox Sensofar, Spain) in a confocal mode with 150 × objective (NA 0.95, maximum slope

71°, vertical resolution <1 nm). The image analysis was done using the SensoMap standard software.

2.4 In vitro pH and conductivity measurements

The in vitro pH variations during soaking in PBS (pH = 7.4) were evaluated by simple immersion test. Briefly, porous scaffolds (about 40 mg) were immersed into 40 mL of PBS at 37 °C. The pH solution was recorded by a pH-meter (WTW, Inolab 720, SenTix 41 electrode) up to 7 days of soaking. The procedure was repeated three times for each specimen and the results were expressed as the mean pH value. Conductivity measurements were carried out by soaking of scaffolds (cca 40 mg) in 40 mL of distilled water at 37 °C. The conductivity was recorded by digital conductometer HANNA HI 9033 equipped with HI 7630 W electrode. The calibration of conductometer was done with 0.1 M KCl solution.

2.5 Water uptake and swelling cement composites

Swelling of composite samples was carried out in 1.5 mL vials by immersion of porous substrates (cca 20 mg) or substrates in the form of films (about 15 mg) to 0.9 % NaCl solution at 37 °C up to constant mass. Soaking was done triplicate for every sample. Swelling was evaluated as ratio of weight of wet sample to this one of origin dry sample.

2.6 Cell cultivation and viability testing

MC3T3E1 mouse preosteoblasts (ECACC, Salisbury, UK) were cultured in culture flasks with surface areas of 75 cm² (SPLLife Sciences, Korea) in MEM (Minimum essential medium) with Earles balanced salts, 2 mM L-glutamine (SAFC Biosciences, Hampshire, UK), 10 % fetal bovine serum (Sigma-Aldrich) and ATB-Antimycotic (Penicillin, Streptomycin, Amphotericin) solution (Sigma-Aldrich). Cells were maintained at 37 °C in 5 % CO₂ atmosphere with 95 % humidity in an incubator (Mettler). The medium was changed every 2 days. After the cells reached about 80 % confluence, they were harvested by trypsinization using 0.25 % Trypsin-EDTA (Sigma-Aldrich) solution followed by the addition of fresh medium to create a cell suspension and the cell numbers were calculated using a Neubauer hemacytometer. Samples were sterilized in an autoclave at 121 °C. The cell proliferation was examined using an MTS test (Cell titer 96 aqueous one solution cell proliferation assay, Promega, Madison, USA). The sterilized scaffolds were placed into the 96-well suspension plate, seeded with 1.0×10^4 cells in 200 μL of complete osteogenic medium alpha modification MEM with 50 μg/mL ascorbic acid, 50 nM dexamethasone and 10 mM β-glycerophosphate (obtained from Sigma) and cultured at

37 °C in atmosphere containing 5 % CO₂ and 95 % humidity in an incubator. The cell proliferation on scaffolds was evaluated for 2 and 10 days after cell seeding. Immediately before the assay, the culture medium was removed from the wells and replaced with fresh medium and the MTS reagent was added. After 2 h of incubation, the intensities of coloring, which characterize the formazan concentration (produced by proliferating cells) in culture medium, were evaluated using a UV–VIS spectrophotometer (Shimadzu) at a wavelength of 490 nm. The measured absorbencies of medium from wells with cell seeded substrates were compared with the ones from wells free of scaffolds in the tissue culture polystyrene plate (treated 96-well tissue culture plate, cellGrade Brand) seeded with cells (1.0×10^4 cells in 200 μ L of complete osteogenic medium). The pure complete culture medium was used as a blank.

The ALP activity of osteoblasts was determined using the phosphatase substrate (Sigma-Aldrich, 5 mg tablet in 5 mL diethanolamine buffer, pH = 9.8). Proliferated osteoblasts were lysed by adding 200 μ L phosphate buffer saline with 0.1 % (v/v) of Triton X-100, 20 mM Tris and 1 mM MgCl₂ to each well, followed by freezing at -20 °C for 1 h and centrifuged at 10,000 rpm for 10 min. Following the 100 μ L phosphatase substrate was added to 100 μ L of cell lysate and the mixture was incubated at 37 °C for 1 h. The alkaline phosphatase reaction was stopped by the addition of 50 μ L of 3 M NaOH. The concentration of p-nitrophenol was determined from a calibration curve using UV/VIS spectrophotometry at 405 nm. The ALP activity was expressed in μ moles of p-nitrophenol produced per 1 min per μ g of DNA. The statistical evaluation of results ($n = 3$) was performed using ANOVA analysis at level $\alpha = 0.05$. The DNA content in samples or control wells after cultivation was evaluated by the fluorescence method (fluorometer Picofluor, Turner Biosystems) with the Hoechst 33258 dye. The calf thymus DNA (Sigma-Aldrich) was used for calibration. The density, distribution and morphology of the MC3T3E1 cells grown on tested discs were visualized with fluorescent live/dead staining (fluorescein diacetate/propidium iodide) by an inverted optical fluorescence microscope (Leica DM IL LED, blue filter).

3 Results

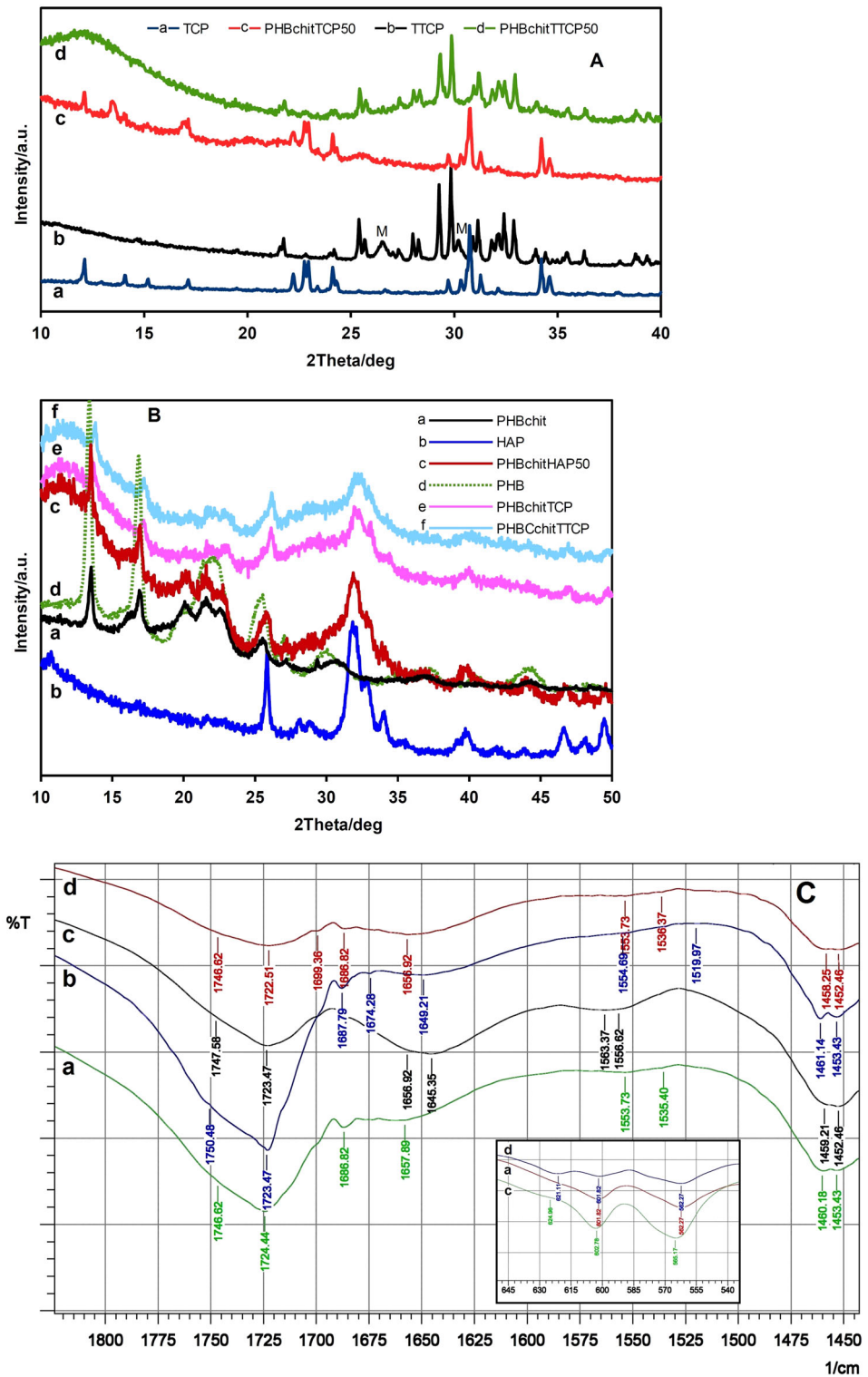
3.1 XRD and FTIR analysis

The XRD patterns as prepared samples with TCP and TTCPMH cement components are shown in Fig 1A. The lines corresponding to starting calcium phosphate phases (TCP (JCPDS 29-0359), tetracalcium phosphate (JCPDS 25-1137), and nanomonetite phase (JCPDS 09-0080)) were

identified in patterns of origin cement powders (Fig. 1A a, b). No newly formed crystalline calcium phosphate phase (like hydroxyapatite) was visible in patterns of composites (Fig. 1A c, d). Despite of the content of nanomonetite phase was significantly reduced in TTCP composite (decrease in intensity of monetite lines) and strongly amorphous regions (between 20–10–15 and 25–35°) of biopolymer components characterized by wide background were observed in the pattern. Note that no lines from the reflections of planes of crystalline PHB component were found in diffractogram (Fig. 1Ad). In the case of TCP composite system, the lower amorphization of biopolymers than in TTCP composite was revealed (especially in PHB biopolymer, which contains a higher fraction of crystalline PHB component (Fig. 1Bd)) as resulted from the comparison of diffractograms by the presence wider and low intense lines at 20–14 and 17° from reflections of (020) and (110) PHB planes of crystalline component [22] respectively and the presence of a low intense background from amorphous parts in biopolymers (Fig. 1Ac). The reduction in PHB crystallinity and the rise in an amount of amorphous phase in PHB/chitosan blends is in accordance with previous results [23]. The formation of nanohydroxyapatite and the fully transformation of origin calcium phosphates in composites after 7 days of soaking in PBS are identified in Fig. 1B, curves c, e, f. The synthesized nanohydroxyapatite (JCPDS 24-0033) (Fig. 1Bb) had a higher crystallinity degree than it was found in all types calcium phosphate composites after setting because of their much larger width of peaks without visible separation of lines in region 2 θ between 30–35°. The biopolymers in cement composites contained higher fraction of amorphous components than in the case of HAP composite. Note that XRD diffractograms of cement composites were practically the same.

FTIR spectra verified vibrations of characteristic functional groups of polyhydroxybutyrate, chitosan and hydroxyapatite in composites after 7 days of soaking in PBS (Fig. 1C). Insignificant changes were found in stretching vibrational mode of C=O group in polyhydroxybutyrate located at 1723 and 1747 cm^{-1} , which correspond to crystalline and amorphous part of PHB respectively [24] and a high fraction of the amorphous PHB component was found in all composite types. The intensity of amorphous band of PHB was higher in TTCP composite. Band arises from amide I vibrations of chitosan at 1656 cm^{-1} was strongly affected by overlapping with vibration of water at 1630 cm^{-1} in hydroxyapatite and amide II vibrations from chitosan in calcium phosphate composites were located at around 1554 and 1536 cm^{-1} whereas the high frequency amide II vibrations were identified in spectra of pure biopolymer blend only [25, 26]. This effect could be related to degradation of the origin chitosan structure with disordering and weakness of hydrogen bonding due to shortening of

Fig. 1 XRD patterns **A** as prepared samples with TCP and TTCPMH cement components; **B** comparison of composites after 7 days soaking in PBS (HAP, PHB, PHB/chitosan—pure starting components). **C** FTIR spectra from vibration of characteristic functional groups of polyhydroxybutyrate, chitosan and hydroxyapatite in composites after 7 days of soaking in PBS (a TCP composite, b PHB/chitosan blend, c HAP composite d TTCP composite)



biopolymer chains by calcium phosphate admixing [27]. In region of wavenumbers between 650 and 540 cm^{-1} , the O–P–O bending ν_4 vibrations of phosphate group and peak from P–OH deformation vibrations in HAP at 630 cm^{-1} were confirmed in spectra of all composites [28, 29]. This

result is in accordance with XRD analysis of samples after soaking where almost full transformation to calcium deficient nanohydroxyapatite was found. Note that no interaction between chitosan and phosphate due to phosphorylation of chitosan were verified by FTIR analysis,

because no peaks from specific P–O–C bending vibrations at 800 cm^{-1} (region without overlapping FTIR bands) were recorded [30].

3.2 Microstructure of scaffolds

The particle morphology of starting TTCPMH and TCP powder precursors is shown in Fig. 2a, b. The TCP powder component was composed of particle agglomerates in the form of mutually interconnected irregular tricalcium phosphate particles with average size around $5\text{ }\mu\text{m}$. Particles had smooth surface texture, which corresponds with a high temperature solid state synthesis and used crushing method (Fig. 2a). In the case of biphasic tetracalcium phosphate/nanomonetite cement mixture, the formation of coarser agglomerates with the fine monetite phase distributed close to origin tetracalcium phosphate particles is clearly demonstrated in Fig. 2b. The average size of agglomerates was about $7\text{ }\mu\text{m}$ and the size of monetite particles did not exceed 100 nm . A large-scale porous microstructure with the high fraction of spherical pores size up to $80\text{ }\mu\text{m}$ was observed in chitosan/polyhydroxybutyrate blend (Fig. 2c). No clearly distinguished or separated individual polymer phases were visible in detail micrograph what confirms good homogeneity of prepared blend. The heterogeneous microstructure was revealed in the HAP composite with wider pore size distribution between $10\text{--}80\text{ }\mu\text{m}$ and a high roughness because of the incorporation of HAP agglomerates to biopolymer blend (Fig. 2d). HAP particles are tightly joined to the smooth biopolymer matrix and no extrapolymer fibres or other polymer objects with different morphology were found in microstructure. A similar type of heterogeneous microstructure as in the last system was observed in Fig. 2e, where the microstructure of TCP cement composite is shown. Contrary to HAP composite, the large spherical pores with dimensions up to $150\text{ }\mu\text{m}$ were visible in microstructure and tricalcium phosphate particles were coated with polymer blend and incorporated into biopolymer matrix. The texture of polymer matrix in TCP cement composite was the same as in HAP composite. Absolutely different microstructure regarding previous two composite types was observed in TTCP cement composite scaffolds (Fig. 2f). The high fraction of small $2\text{--}4\text{ }\mu\text{m}$ spherical pores and a low number of about $50\text{ }\mu\text{m}$ pores can be found in microstructure what give composite scaffold the spongy-like character. No visible calcium phosphate particles were identified in microstructure. For demonstration of calcium phosphate particles distribution in composites and the better distinction of calcium phosphates in microstructures, the EDX mapping of elements on surfaces of samples was done. From the comparison of maps in Fig. 2g, where the distribution of calcium and phosphorus in composites is revealed, resulted the relatively homogeneous

distribution of calcium phosphates in all samples. The coarser particle agglomerates were found in HAP and TCP composites contrary to both the partially particle disaggregation and a more homogeneous distribution of calcium phosphate particles demonstrated in the spongy-like microstructure of TTCP cement composites.

The changes in particle morphology and microstructure of composite scaffolds were verified after 7 days soaking in PBS solution (Fig. 3). The surface of HAP composites was coated with continuous calcium phosphate layer composed of extremely fine nanosized apatite-like particles (Fig. 3a). On the other hand the very thin (a few tens nanometers) agglomerates of plate-like hydroxyapatite particles up to $5\text{ }\mu\text{m}$ length were precipitated during the transformation of TCP (Fig. 3b) or TTCPMH (Fig. 3c) cement components in composites. The high surface roughness is demonstrated in images of these scaffolds, where the thin edges of plate-like particles were oriented out of sample surface (almost perpendicularly to surface).

The surface textures of the PHB/chitosan and composite films prepared from 14 days enzymatically degraded scaffolds are shown in Fig. 4. Relatively smooth texture ($S_a = 0.56$; $S_q = 0.67\text{ }\mu\text{m}$) with long irregular narrow microcracks was found on PHB/chitosan films (Fig. 4a). The roughness of HAP composite films was a bit smaller ($S_a = 0.40$ and $S_q = 0.52\text{ }\mu\text{m}$) than that of pure biopolymer films. Non porous texture with long fiber-like objects with thickness does not exceed $5\text{ }\mu\text{m}$ and irregularly shaped objects standing out from surface were visible in HAP films (Fig. 4b). EDX map from this sample clearly indicated that the extending surface and uniformly distributed objects characterize regions with the higher density of hydroxyapatite particles, which are not good interconnected with biopolymer matrix after pressing. In the case of TTCP composite films, the texture was composed of separated regions of calcium phosphate phase (white objects) and biopolymer blend region as it was verified by EDX map (Fig. 4c). The surface of TTCP film was smoother ($S_a = 0.13$; $S_q = 0.17\text{ }\mu\text{m}$) than HAP film, non porous microstructure with few very thin short microcracks at boundaries between calcium phosphate particles and biopolymer matrix were observed. Approximately double values of roughness parameters were measured in TCP composite films than HAP films ($S_a = 0.25$; $S_q = 0.32\text{ }\mu\text{m}$). None sharply microscopically distinguished regions with pre-concentrated calcium phosphate and biopolymer phases were identified on surface of TCP films. Despite of two different types of texture were found in films. The EDX analysis showed that almost pure biopolymer regions are represented by rougher and rounded surface objects with the large number of very short and thin microcracks displaced between globular extremely fine biopolymer particles (Fig. 4d).

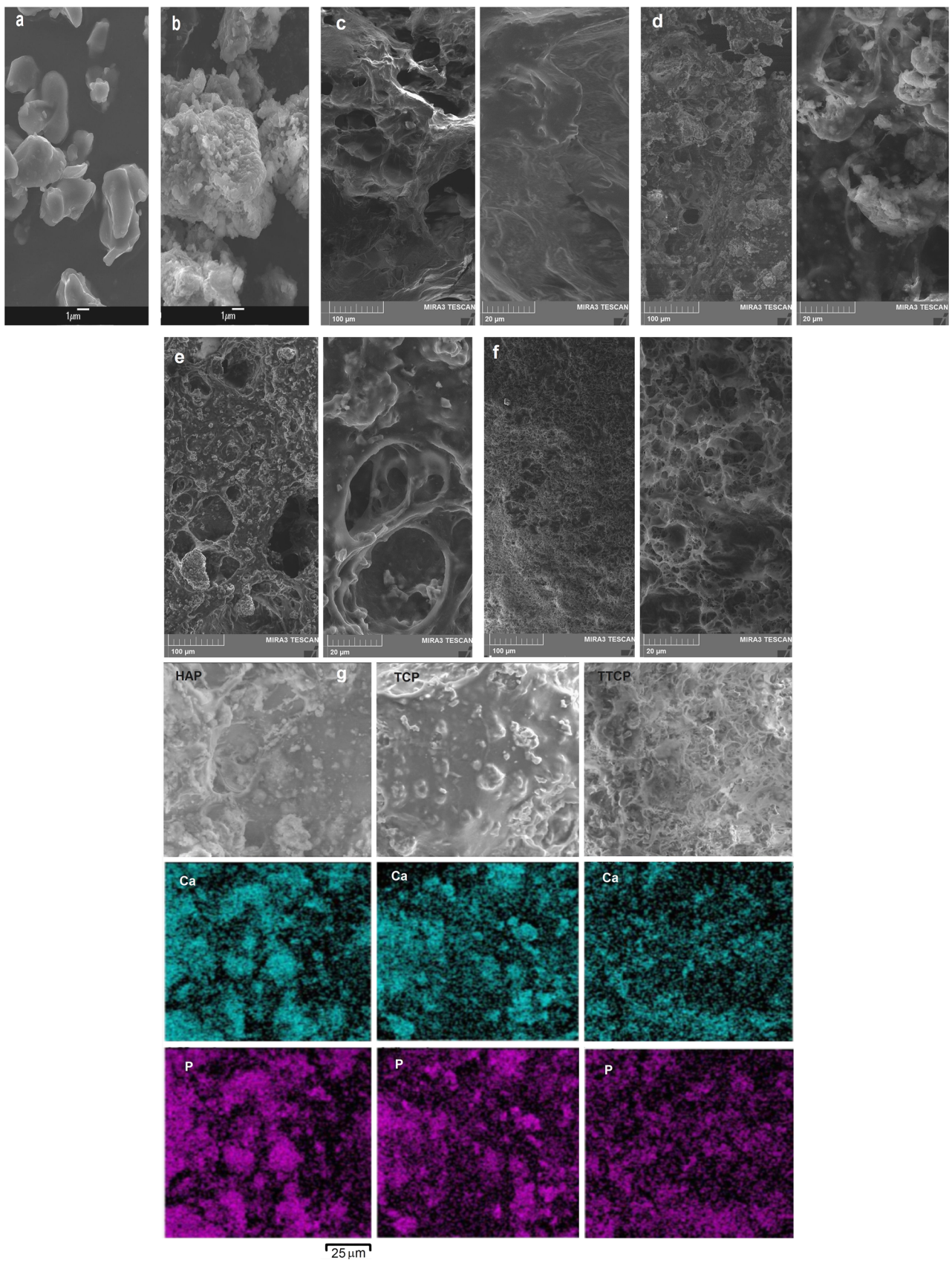


Fig. 2 Particle morphology of starting TCP (a) and TTCPMH (b) powder precursors, microstructure of composite scaffolds (c PHB/chitosan blend, d HAP composites, e TCP composites, f TTCP composites) and EDX mapping of Ca and P elements distribution in composite scaffolds (g)

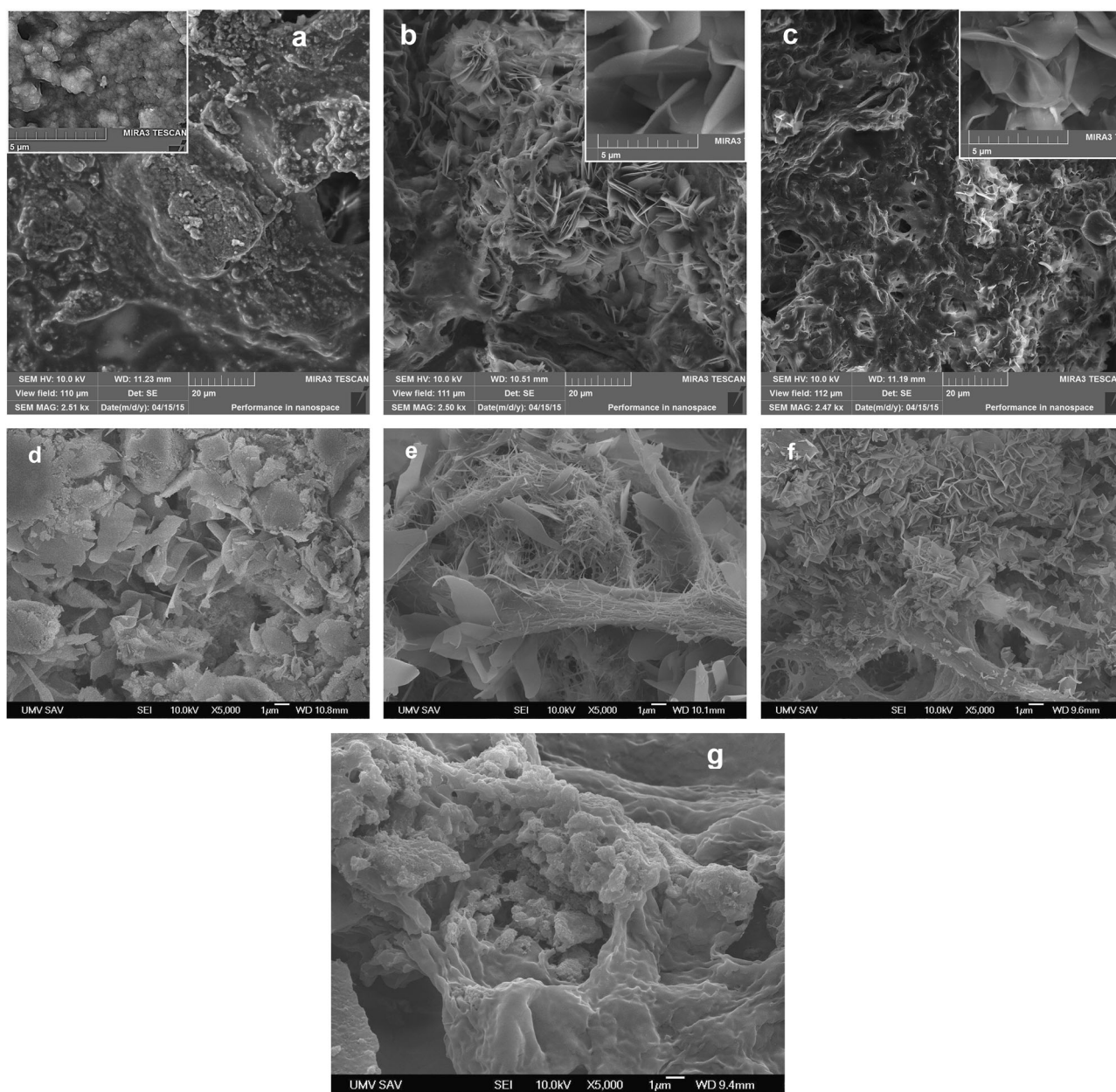


Fig. 3 Particle morphology and microstructure of composite scaffolds after 7 days soaking in PBS solution (**a** HAP composites, **b** TCP composites, **c** TTCP composites), microstructure details of

enzymatically degraded scaffolds after 14 days of treatment in PBS/lysozyme solution at 37 °C (**d** PHB/chitosan blend, **e** HAP composites, **f** TCP composites, **g** TTCP composites)

3.3 pH and conductivity changes during composite soaking, lysozyme degradation of chitosan

In Fig. 5, the dependences of both the pH of PBS and conductivity of water on soaking time of composite scaffolds are shown. Practically the same dependences with small changes in pH values were measured during soaking of PHB/chitosan blend, HAP and TCP composite scaffolds. On the other hand, the rapid rise in pH values up to 9 was revealed during first 48 h (with maximum at about 100 h) of

TTCP composite scaffold soaking in PBS at 37 °C. The gradual pH decrease was found after 150 h of soaking but the pH around 9 was still measured after 14 days (336 h). The conductivity of water was insignificantly changed during soaking of the biopolymer blend. A slowly increase in conductivity up to 120 μS without any changes with prolonged time period was observed in suspension with HAP composite. A gradual rise in conductivity up to 330 μS was confirmed during soaking of TCP composite and conductivity close to maximal value was stabilized approx.

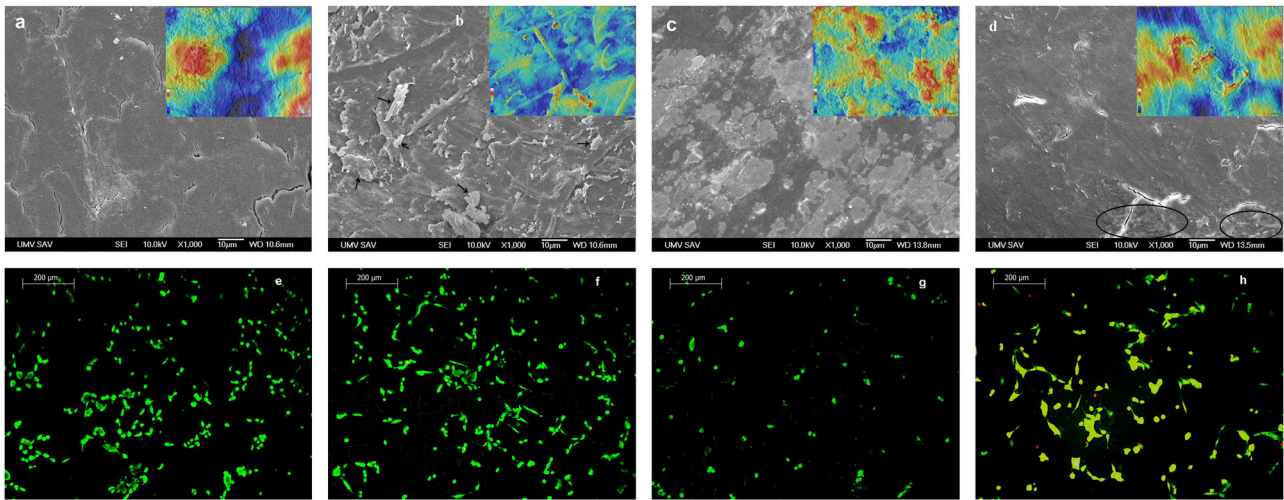


Fig. 4 Surface textures of composite films prepared from 14 days enzymatically degraded scaffolds and altitude surface distribution (in detail) (a PHB/chitosan film, b HAP film (arrows mark hydroxyapatite particles), c TTCP film (bright regions represent calcium phosphate phase), d TCP film (circles define regions with pure biopolymer

blend); morphology of osteoblasts on untreated composite film surfaces after 48 h of culture in incubator at 37 °C, 5 % CO₂ and 95 % humidity (e PHB/chitosan blend, f TCP film, g HAP film, h TTCP film)

after 160 h of soaking. The dependence of conductivity of TTCP water suspension on soaking time had similar character as in the case of pH measurement. Thus, the maximum conductivity (~520 μS) was observed after 100 h with following decrease (~280 μS) after 210 h of soaking and conductivity was stabilized on this value.

Enzymatic lysozyme degradation of chitosan in composite scaffolds in PBS/lysozyme solution at 37 °C was evaluated via measurement of RES, which are produced due to the degradation and shortening of chitosan chains. About triplicate rise in the content of RES in biopolymer blend was shown after 3 days of degradation (Fig. 6a) with following an insignificant change in RES content after 14 days and fast rise after 31 days of degradation in this system. In the case of calcium phosphate composites, a small increase in amount of RES was identified with soaking time in lysozyme solution up to 31 days. Note that the total reduction in scaffold weights after lysozyme treatment did not exceed 2 % and it was independent on composition of composites. The changes in distribution of chitosan average molecular weight (Mw) after 3 days of enzymolysis of samples were evaluated by GPC chromatography. From the comparison of Mw in composite scaffolds (Fig. 6b) resulted the reduction in Mw of origin biopolymer even unaffected by lysozyme attack. The strong effectivity of lysozyme to chitosan degradation was verified after 3 days of soaking when Mw were lowered and close to 3–5 kDa.

The microstructure details of enzymatically degraded scaffolds after 14 days of treatment are depicted in Fig. 3. The strong degradation of chitosan in pure biopolymer blends characterizes the formation of separated thin plate-like particles with size up to 5 μm due to debonding and

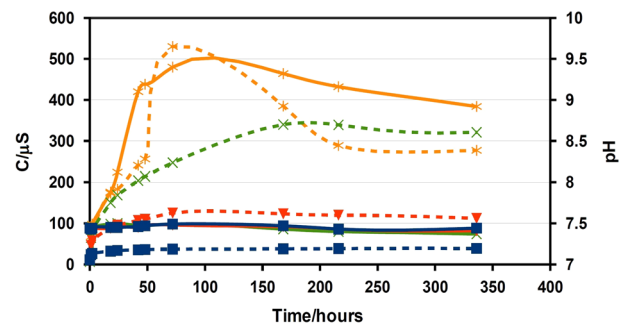
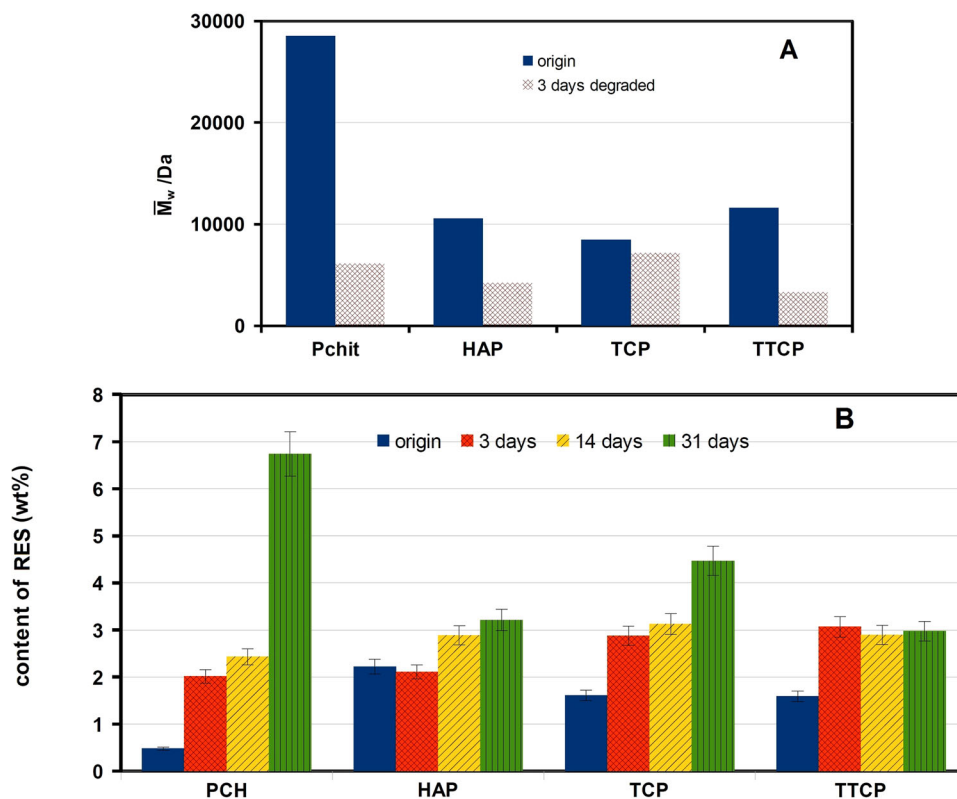


Fig. 5 Changes in pH of PBS (solid lines) and conductivity of water (dashed lines) during soaking of composite scaffolds (Black triangle PHB/chitosan, inverted red triangle HAP composite, cross symbol TCP composite, asterisk TTCP composite)

disruption of chitosan chains (Fig. 3d) with damaging of the original smooth morphology of scaffold surface (Fig. 2c). Very fine deposits of calcium phosphate phase are visible in the image. In the microstructure of lysozyme treated HAP composite scaffolds, similar large plate-like biopolymer particles were visible commonly with the long thin fibre-like hydroxyapatite particles precipitated on the surface of biopolymer plates or fibres (Fig. 3e). The high number of hydroxyapatite particles (1 μm in size) with the same plate-like morphology like had chitosan particles after enzyme degradation was found in the microstructure of TCP scaffolds (Fig. 3f). Different character of microstructure was visible in TTCP composite scaffolds, where plate-like polymer particles were not identified probably as the result of their thicker compact calcium phosphate coating after the cement component transformation (Fig. 3g). Note

Fig. 6 a Average molecular weights of chitosan in origin scaffolds and after enzymatic lysozyme degradation of chitosan in composite scaffolds after 3 days in PBS/lysozyme solution at 37 °C, **b** Content of RES in composite scaffolds after enzyme degradation in PBS/lysozyme solution at 37 °C



that the long biopolymer fibres were clearly observed in all composite microstructures and the scaffold structures were more opened.

3.4 Water uptake and swelling of porous substrates and composite films

The differences in water uptake or swelling between porous and non-porous (film) substrates are shown in Fig. 7, where the final water uptake at a constant mass of samples is demonstrated. The fast swelling was revealed after first 2 h of soaking when the mass increments even achieved about 90 % of the final water uptake and the constant mass of samples was found after 2 days of swelling. The mass increment of porous substrates is composed of two main components—the change in mass due to solution uptake (0.9 % NaCl) into porous microstructure and swelling of biopolymer matrix. As resulted from image, almost the same weight changes were found after 48 h soaking of composite films whereas the mass increment of biopolymer film was bit higher (about 20 % difference). From comparison of scaffolds and film substrates results that in the case of biopolymer and HAP scaffolds, about 50 % of mass increment arised from solution uptake in pores. The weight changes of all lysozyme treated films except HAP film were comparable and independent on enzyme degradation (statistically insignificant differences, $P > 0.40$). The mass

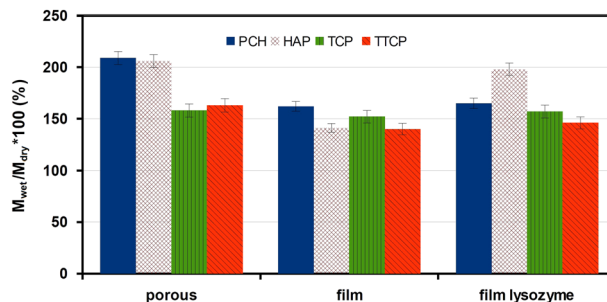


Fig. 7 Differences in water uptake or swelling between porous and non-porous (film) composite substrates

increments (around 80 % higher than in other films) of degraded HAP composite films were the same like in porous HAP scaffolds.

3.5 Attachment and morphology of osteoblasts on film surfaces, proliferation and osteoblast ALP activity on composites

The proliferation of osteoblasts on porous composite scaffolds is shown in Fig. 8. From comparison resulted that the most intense proliferation and population growth of cells were found on scaffolds based on biopolymer blend and the viability reached about 60 and 75 % of standard after 2 and 10 days respectively. The cell proliferation on TCP and

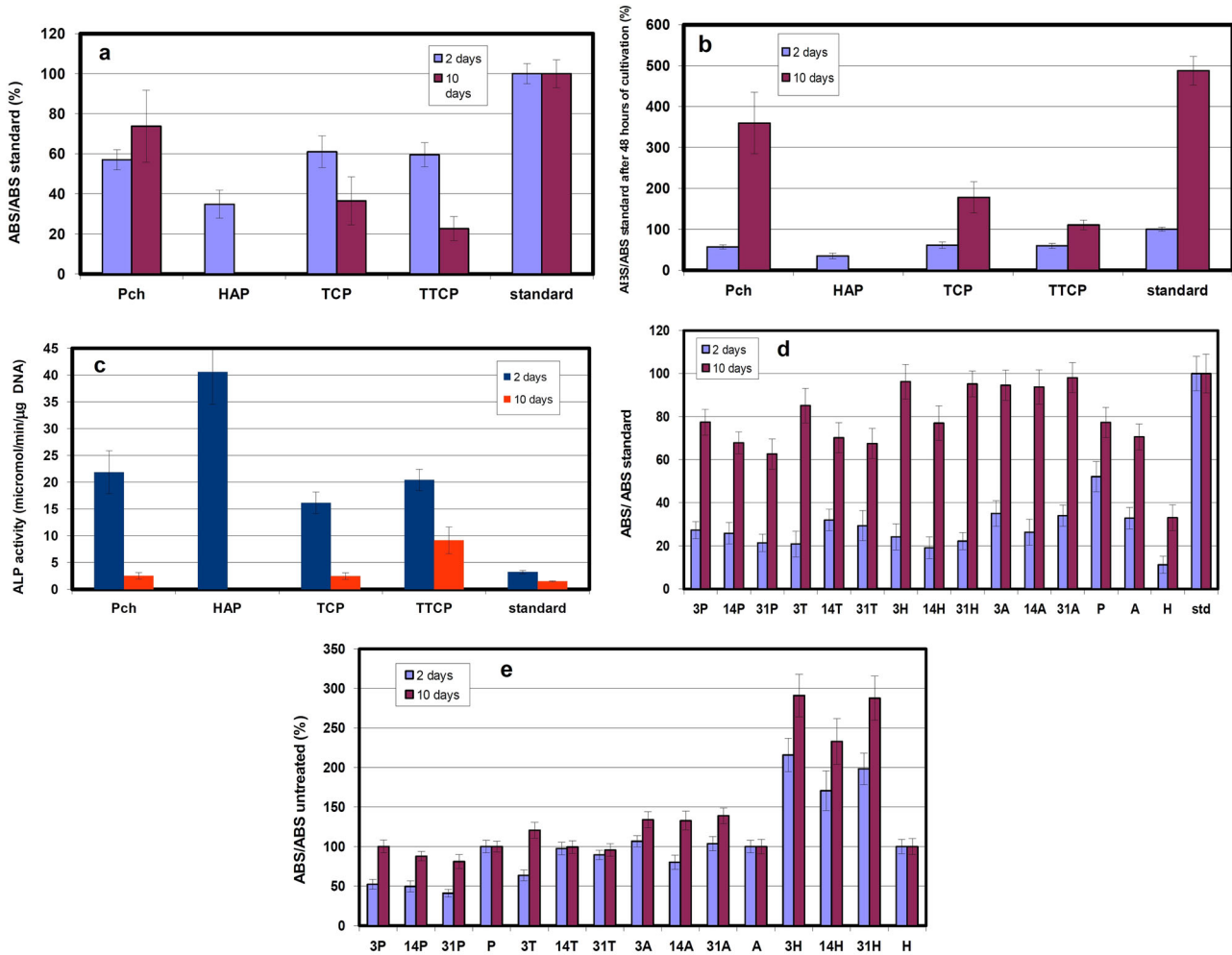


Fig. 8 Proliferation of osteoblasts on porous composite scaffolds in relation to standard at given time of culture (a) and to standard after 48 h of cultivation (b), ALP activity of osteoblasts; proliferation of osteoblasts on composite films in relation to standard at given time of

culture (c) and to proliferation on untreated films of each composite type (d) (A-TCP films (numbers sign the time of degradation), T-TTCP films, H-HAP films, P-PHB/chitosan films)

TTCP composite scaffolds was the same after 48 h of culture (approx. 60 % of standard) and the cell viabilities after 10 days of cultivation (Fig. 8a) on both scaffold types were much lower than 70 % level, which represents limity for enhanced cytotoxicity of evaluated biomaterial (EN ISO 10993-5). Despite of above facts, the rise in population of osteoblasts was verified with the prolongation of cell cultivation on cement composite scaffolds (Fig. 8b) but the growth in cell number was slower than in the case of biopolymer scaffolds or standard. No viability was measured on the HAP composite after 10 days of culture, thus, this scaffold was severe in vitro cytotoxic for osteoblast cell line. The ALP osteoblast acivity was significantly enhanced on both cement composites after 2 days of cultivation and it was higher on the biopolymer scaffolds than on standard polystyren microplate (Fig. 8c).

Absolutely different behavior of cells was demonstrated on composite films prepared by the simple pressing in steel

mould. The osteoblast attachment and cell morphology on film surfaces after 48 h of culture in incubator at 37 °C, 5 % CO₂ and 95 % humidity are documented in Fig. 4e–h. The high density of osteoblasts was observed on the biopolymer blend (Fig. 4e) and despite of the similar cell distribution on TCP composites (Fig. 4f), the more prolonged shape of cells with visible filopodia was found on composite films. A lower density of osteoblasts with spherical morphology was confirmed on HAP composite films (Fig. 4g). Note that no dead cells (red color) were identified on above type of samples. On the other hand, better spreading of osteoblasts characterized by the occupation of a larger area on film surfaces with longer mutually interconnected filopodia was revealed on TTCP composite films (Fig. 4h). The few dead cells were observed on surface of this sample.

The lowest proliferation activity of osteoblasts was measured on lysozyme treated HAP composite films and did not exceed 10 % of the cell proliferation on standard. In

comparison with HAP scaffolds, the proliferation was even lower after 2 days of cultivation but it rose after 10 days of culture and achieved about 35 % proliferation on standard. A statistically much higher proliferation was found on degraded biopolymer films (~50 %) than cement composite films (~35 %) after 2 days of culture and the population growth of cells was faster on cement composite films (Fig. 8d) (statistically insignificant difference after 10 days of cultivation, $P > 0.1711$). Very similar proliferation activity of osteoblasts was identified after 48 h of culture on all surfaces of lysozyme treated films (around 22–35 % of standard) irregardless degradation period. From Fig. 8d results that the fast population growth was verified mainly on treated HAP and TCP composite films with almost 95 % proliferation in relation to control after 10 days of cultivation. Thus the cytotoxicity of HAP and TCP treated composite films was very low after prolonged cultivation contrary to the moderate cytotoxicity of TTCP and biopolymer composites, on which the cell proliferation reached about 65–70 % proliferation of standard. The relative proliferations of cells calculated as formazan concentration produced by cells on lysozyme treated films relatively to this one on untreated films are documented in Fig. 8e. Statistically significant effect ($P < 0.0001$) of lysozyme treatment on cell proliferation was demonstrated in the case of HAP composite films where approx. 200 and 300 % increase in proliferation activity independently on degradation time was found in relation to untreated films. About 20 % enhancing of cell proliferation activity was observed on treated TCP composite films compared to untreated one (statistically significant difference, $P < 0.0002$). The proliferation on treated biopolymer films was reduced during first 48 h of cultivation irregardless time of enzymolysis with following rise to values close to that of untreated film (no difference, $P > 0.8815$) after 10 days of culture. No effect of lysozyme treatment on osteoblast proliferation activity was confirmed on TTCP composite films.

4 Discussion

The composite calcium phosphate scaffolds were prepared by the simple preparation procedure without accent on disaggregation of agglomerates generally present in powder solid nanophases like nanohydroxyapatite or cement calcium phosphate mixtures with nanosized component. The motivation for using of such an experimental method was the fact that there are insufficient informations about behaviour of osteoblasts on polyhydroxybutyrate/chitosan composites reinforced with various calcium phosphates and secondly, to show some view on the effect of substrate microstructure and lysozyme degradation of chitosan in substrates on osteoblast response. From comparison of

scaffold microstructures and evaluation of their influence on osteoblast proliferation resulted that despite of similar microstructural character of HAP and TCP scaffolds characterized by the larger pores and homogeneously distributed calcium phosphate agglomerates, absolutely different cell behaviour on these scaffolds was observed. On the other hand, contrary to the finer pore structure details in TTCP scaffolds than in TCP scaffolds, the same proliferation of osteoblasts after 48 h was measured. These facts clearly demonstrate that the pore size distribution does not play the main role in explanation of different osteoblast response in composite scaffolds after 48 h of culture and it could be to have a some influence with prolonged culture only because the population growth of osteoblasts was slower on TTCP than on TCP scaffolds. The extremely values of pH during the cultivation due to transformation of the cement phases represent the second parameter, which could be affect the cell viability. Note that pH values of PBS solution after immersion of biopolymer scaffold, HAP and TCP composite scaffolds were almost equal to starting pH of PBS (7.4) and they were practically unchanged during 14 days of soaking whereas the rapid rise in pH solution (up to 9.5) after TTCP scaffold immersion was confirmed. Variations in pH solution after immersion of various calcium phosphates depend on transformation mechanism of cements, where dissolution/precipitation mechanism characterizes processes in TTCP/nanomonetite cements and hydrolysis in the case of TCP cement are main processes. As it can be seen in Fig. 5, the gradual rise in conductivity of solution during soaking of TCP scaffold is characteristic for slowly hydrolysis and the transformation connected with diffusion of ions contrary to rapid increase of the solution conductivity after immersion of TTCP sample due to dissolution and hydrolysis of both cement phases and following interaction of ions with precipitation of nanohydroxyapatite. The final phase in cement composites represents a similar type of calcium deficient hydroxyapatite (with similar values of solubility constants), which verify very close values of conductivity after fully transformation of cement components. Despite of insignificant changes in pH and the lowest rise of ionic concentration in solution with the HAP composite scaffold, the proliferation of osteoblasts during first 48 h was only half than on other scaffolds, thus, the large pH changes (to basic region) in culture medium were not responsible for weak proliferation of cells on composite scaffolds. Note that the number of osteoblasts on substrates during starting culture period after cell seeding on substrates depends mainly on adherence of cells to surface of substrate because no extracellular matrix with integrins is still present on scaffolds and cells have to adapt to substrate or on cultivation conditions. In the next stage, the cell adherence can be strongly affected by the cell secretion of extracellular matrix at substrate surface or to culture medium, where the

concentration of specific proteins increases with time at proper conditions. The surface of composite substrates was significantly modified by the precipitation of extremely fine calcium deficient hydroxyapatite particles in the form of more compact coating on HAP scaffolds or by the formation of plate-like agglomerates of nano-hydroxyapatite particles on cement composite scaffolds. It was demonstrated that the adsorption of proteins from medium increased with the crystallinity of hydroxyapatite particles [31] and the coarser plate-like nanohydroxyapatite particles improved the proliferation activity of osteoblasts and supported expression of mature osteogenic markers because of the differential cell responses to subtle changes in the apatite microenvironment [32]. The higher pre-adsorbed amounts of extracellular matrix proteins and serum proteins on hydroxyapatite substrates supported the cell attachment and cell proliferation [33]. Besides the cell apoptosis of osteoblasts was enhanced by cell contact with the coarser rod-like hydroxyapatite particles (200 nm in length and 50 nm in diameter) in contrast with the cell growth and the inhibition of cell apoptosis by fine 20 nm spherical nanohydroxyapatite particles [34]. Similarly the precipitation of the extremely fine calcium phosphate coating on the surface of hydroxyapatite ceramics in the complete culture medium demonstrated markedly improved osteoblast adherence and proliferation during cultivation [35] contrary to insignificant differences between the initial cell attachment and the proliferation of osteoblasts on hardened CPC or sintered hydroxyapatite samples. Despite of the nanocrystalline CPC samples had a more enhanced differentiation potential than crystalline hydroxyapatite samples [36]. On the other hand, the reason for the observed enhanced cytotoxicity of the nanohydroxyapatite could be the change in osmotic pressure of the culture medium after release of water from the nanocrystalline lattice [37]. It was shown the suppression in the cell proliferation on fine nanoneedles or nanofibers in contrast to good cell growth on the smoother large grains or substrates consisting of wide nanosheets [38]. From measurement of osteoblast proliferation on composite scaffolds resulted that the gradual precipitation of fine calcium phosphate deposits on HAP scaffolds did not help to improve the adherence or viability of osteoblasts on substrates with cultivation time because no live cells were found after 10 days of culture on HAP substrates. On the other hand, the population of osteoblasts rose with culture time on TCP and TTCP cement scaffolds (containing plate-like hydroxyapatite agglomerates even with lower or the same crystallinity like in the case of HAP scaffolds) although slower than on biopolymer substrates or control. It may be speculated that swelling or water uptake in scaffolds could be positively affect the viability of cells due to improving the flow of nutrition to cells but the HAP scaffolds had much higher

swelling than other composite scaffolds. It is clear that amorphous or nanocrystalline character of hydroxyapatite phase in composite substrates was not the reason for poor proliferation activity of osteoblasts or cell dead on HAP composite scaffolds. We believe that the crucial role on proliferation and viability of osteoblasts had the different microtopography of surfaces in scaffolds characterized e.g. by defined porosity, proper morphology of hydroxyapatite particles or agglomerates and their distribution in scaffolds. For elimination of the influence of porosity or different pore distribution and the large topographic differences between individual composite scaffolds, the scaffolds (treated or untreated with lysozyme) were pressed under same conditions to form of films. This method allowed studying direct effect of lysozyme degradation of chitosan in composites on osteoblast behaviour.

The strong influence of the calcium phosphate addition to polyhydroxybutyrate/chitosan blend on average molecular mass of chitosan was verified in Fig. 6, where almost triplicate decrease in M_w of chitosan in untreated composite scaffolds and the content of reducing sugar ends (RES) respectively in comparison with biopolymer blends were found. The lysozyme is effective enzyme for the degradation of chitosan with partially acetylated amino group [39]. The chitosan enzymatic hydrolysis by lysozyme is influenced by the proper distribution of N-acetylated groups in chitosan chains, which are binding to active sites of enzyme [40, 41]. Enzyme degradation by lysozyme during 3 days caused further reduction in M_w of chitosan in all samples with insignificant changes in an amount of RES because the high molecular mass chains of chitosan were degraded during this stage. The content of RES gradually rose with time of enzymolysis in biopolymer blend, HAP and TCP scaffolds while no changes were revealed in TTCP composite scaffolds. It is clear that the microstructure of biopolymer scaffolds was more opened to action of lysozyme and the formation of hydroxyapatite coating in any form at sample surfaces (including inner surfaces of pores) significantly hinder to the access of enzyme to chitosan in composite scaffolds. The rapid rise in pH of lysozyme solution containing the TTCP substrate caused decrease in lysozyme activity, which is maximal at pH around 6.2 [42]. Besides the dense calcium phosphate coating was formed on the substrate. These effects were the reason for no rise in RES in TTCP sample with enzymolysis time. The presence of plate-like biopolymer particles with exception of TTCP composite scaffolds, where the more compact hydroxyapatite layer was created on pore surfaces, demonstrated the degradation of chitosan fibers in scaffolds. The results from measurement of proliferation activity of osteoblasts on films clearly showed different response than on scaffolds. The statistically reduced viability of osteoblasts on all composite films in comparison with scaffolds was observed

after 2 days of cultivation. No effect on cell proliferation was found on untreated biopolymer films while the proliferation on untreated HAP films was strongly suppressed ($P > 0.2242$). This evidenced, that porosity of calcium phosphate composites plays the positive role on the osteoblast adherence and proliferation during a short time period after cell seeding. The rapid population growth of osteoblasts was found on all untreated films after 10 days of culture with about 70 % viability relatively to control. In the case of untreated HAP film, viability of osteoblast did not exceed 40 % of control and the film could be still characterized as severe cytotoxic. Note that it can be seen difference between behaviour of osteoblasts on scaffolds and films, where the stronger cell growth was observed after 10 days of culture. It is possible to assume that the surface roughness could be affect on adherence and proliferation of osteoblast during first 48 h of culture but for example differences between roughness of individual lysozyme treated films were not so large (S_a in region 0.13–0.56 μm , HAP films had the highest roughness from other composite films) and besides, no clearly dependence of the cell viability on roughness was identified. It was found that larger differences in S_a of hydroxyapatite ceramics from 0.78 to 2.86 μm caused about 15–20 % change in proliferation of osteoblasts [43] and the same proliferation of osteoblasts was measured on surfaces of micro- or nano- hydroxyapatite loaded polyhydroxybutyrate films [44]. On the other side, extremely small variances in surface roughness (in nanoscale level) of polyhydroxybutyrate/hydroxyapatite films caused around 30 % increase in ALP activity of osteoblasts [45]. No correlation between swelling films and osteoblast proliferation was measured too. The effect of lysozyme degradation of chitosan in composites demonstrates Fig. 8d, where the proliferation of osteoblasts on treated films is compared relatively to that of untreated films. The significant enhancing of cell viability was revealed on treated HAP films after both evaluated culture period. The statistically significant rise in viability of osteoblasts was found on treated TCP films compared with untreated films after 10 days of cultivation. Note that no dependence of cell viability on time enzymolysis was confirmed in the case of HAP or TCP films and probably the confluence of cells was achieved on these substrates after 10 days of culture. None or a small decrease in proliferation of osteoblasts were measured on treated TTCP and biopolymer films respectively, thus the presence of LMWC in treated biopolymer films had insignificant effect on cell viability. The enhanced swelling was evidenced in the lysozyme treated HAP films, which was comparable with water uptake and swelling of porous HAP scaffolds. Because of none such an effect was measured in other samples including biopolymer films, this fact demonstrates that synergistic effect of nanohydroxyapatite particles with

a high specific surface, incorporated to starting composite mixture and the low molecular weight chitosan produced by lysozyme degradation support swelling of composites. Note that no dependence of cell viability with enzymolysis time was found on treated composite films. No reduction in viability of cells and rise in antimicrobial activity were showed on polyhydroxybutyrate-co-valerate/chitosan composite films [46]. It was revealed that the low molecular water soluble chitosans caused a significant increase in ALP, cell viability, and mineralization of osteoblastic cells [11]. A small decrease in viability (10–20 %) of osteoblasts was observed in biomimetically precipitated calcium phosphates in chitosan solution [47]. The enhanced osteoblast cytotoxicity was revealed on CPC/low molecular chitosan composites with M_w equal 3 and 20 kDa [9]. From above analysis resulted that the synergistic effect of uniformly distributed nanohydroxyapatite particles, proper surface micro- or nano- topography and the presence of LMWC in HAP composite films practically compensated the cytotoxicity of origin untreated films or scaffolds. If compare HAP scaffolds and films, a much higher roughness and different topography of pore surfaces in scaffolds due to presence of hydroxyapatite agglomerates is clearly evidenced what can play the crucial role in severe cytotoxicity of scaffolds. Besides the strong swelling of treated HAP films probably significantly changed the film surface topography and following the cell adherence to films as resulted from comparison of cell viabilities on both HAP film types.

5 Conclusions

The adherence and proliferation of osteoblasts on biopolymer and cement composite scaffolds during first 48 h from cell seeding were good and viability of osteoblasts achieved around 60 % of control. The slower population growth of cells on composites than on biopolymer scaffolds was observed in following culture period up to 10 days and the strong cytotoxicity of HAP composite scaffolds composed of agglomerates of nanohydroxyapatite particles was revealed. After elimination of the effect of substrate porosity, microstructure and texture parameters on osteoblast proliferation by pressing of scaffolds to film form, the cell growth and viability of osteoblasts on films were significantly enhanced with prolongation of culture but the cytotoxicity of lysozyme untreated HAP films was still much higher than that of other composite films. It was evidenced that the porosity of composites plays positive role on osteoblast adherence and proliferation during a short time period after cell seeding. No cytotoxicity of treated composite films prepared from lysozyme degraded scaffolds, which contained LMWC, was revealed after 10 days

of cultivation. The faster population growth of osteoblasts was found on treated HAP films, which supports opinion that the synergistic effect of distribution and morphology of nanohydroxyapatite particles, proper surface micro- or nano- topography and mainly the presence of LMWC in HAP composite films were responsible for compensation of the cytotoxicity of origin untreated HAP films or scaffolds.

Acknowledgments This work was supported by the Slovak Grant Agency of the Ministry of Education of the Slovak Republic and the Slovak Academy of Sciences, Project No. 2/0047/14 and within the framework of the project “Advanced implants seeded with stem cells for hard tissues regeneration and reconstruction”, which is supported by the Operational Program “Research and Development” financed through the European Regional Development Fund.

Compliance with ethical standards

Conflict of interest The authors declare that they have no conflict of interest

References

- Muzzarelli R, Baldassarre V, Conti F, Ferrara P, Biagini G, Gazzanelli G, Vasi V. Biological activity of chitosan. Ultrastructural study. *Biomaterials*. 1988;9(3):247–52.
- Thein-Han WW, Misra RDK. Biomimetic chitosan–nanohydroxyapatite composite scaffolds for bone tissue engineering. *Acta Biomater*. 2009;5:1182–97.
- Kong L, Gao Y, Lu G, Gong Y, Zhao N, Zhang X. A study on the bioactivity of chitosan/nano-hydroxyapatite composite scaffolds for bone tissue engineering. *Eur Polym J*. 2006;42:3171–79.
- Siddiqui N, Pramanik K, Jabbari E. Osteogenic differentiation of human mesenchymal stem cells in freeze-gelled chitosan/nano β -tricalcium phosphate porous scaffolds crosslinked with genipin. *Mater Sci Eng C*. 2015;54:76–83.
- Seda Tıglı R, Karakeçili A, Gümüşderelioglu M. In vitro characterization of chitosan scaffolds: influence of composition and deacetylation degree. *J Mater Sci Mater Med*. 2007;18:1665–74.
- Hesarakı S, Nezafati N. In vitro biocompatibility of chitosan/hyaluronic acid-containing calcium phosphate bone cements. *Bioprocess Biosyst Eng*. 2014;37:1507–16.
- Hockin XuHK, Simon CG. Fast setting calcium phosphate–chitosan scaffold:mechanical properties and biocompatibility. *Biomaterials*. 2005;26:1337–48.
- Lee JS, Baek SD, Venkatesan J, Bhatnagar I, Chang HK, Kim HT, Kim SK. In vivo study of chitosan-natural nano hydroxyapatite scaffolds for bone tissue regeneration. *Int J Biol Macromol*. 2014;67:360–66.
- Wu W, Hua X, He Z, Wang X, Yu X, Ren W. The bactericidal and biocompatible characteristics of reinforced calcium phosphate cements. *Biomed Mater*. 2012;7:045003. doi:10.1088/1748-6041/7/4/045003. (10pp)
- Mellegård H, Strand SP, Christensen BE, Granum PE, Hardy SP. Antibacterial activity of chemically defined chitosans: Influence of molecular weight, degree of acetylation and test organism. *Int J Food Microbiol*. 2011;148:48–54.
- Hou JW, Qian L, Kou JM, Zhang CW, Jia XJ, Tian W. Effect of water-soluble chitosan on the osteoblast function in MC3T3-E1 cells. *Int J Biol Macromol*. 2015;72:1041–43.
- Jack KS, Velayudhan S, Luckman P, Trau M, Grøndahl L, Cooper-White J. The fabrication and characterization of biodegradable HA/PHBV nanoparticle-polymer composite scaffolds. *Acta Biomater*. 2009;5(7):2657–67.
- Tai HY, Fu E, Cheng LP, Don TM. Fabrication of asymmetric membranes from polyhydroxybutyrate and biphasic calcium phosphate/chitosan for guided bone regeneration. *J Polym Res*. 2014;21:421. doi:10.1007/s10965-014-0421-8
- Sadat-Shojai M, Khorasani MT, Jamshidi A, Irani S. Nano-hydroxyapatite reinforced polyhydroxybutyrate composites: A comprehensive study on the structural and in vitro biological properties. *Mater Sci Eng C*. 2013;33:2776–87.
- Cool SM, Kenny B, Wu A, Nurcombe V, Trau M, Cassady AI, Grøndahl L. Poly(3-hydroxybutyrate-co-3-hydroxyvalerate) composite biomaterials for bone tissue regeneration: In vitro performance assessed by osteoblast proliferation, osteoclast adhesion and resorption, and macrophage proinflammatory response. *J Biomed Mater Res*. 2007;82A:599–610.
- Zheng Y, Wang Y, Yang H, Chen X, Chen Z. Characteristic comparison of bioactive scaffolds based on polyhydroxyalkoanate/bioceramic hybrids. *J Biomed Mater Res Part B Appl Biomater*. 2007;80B:236–43.
- Cheung MK, Wan KPY, Yu PH. Miscibility and morphology of chiral semicrystalline poly-(R)-(3-hydroxybutyrate)/chitosan and poly-(R)-(3-hydroxybutyrate-co-3-hydroxyvalerate)/chitosan blends studied with DSC, 1H T1 and T1q CRAMPS. *J Appl Polym Sci*. 2002;86:1253–58.
- Ikejima T, Inoue Y. Crystallization behavior and environmental biodegradability of the blend films of poly(3- hydroxybutyric acid) with chitin and chitosan. *Carbohydr Polym*. 2000;41:351–56.
- Veleirinho B, Coelho DS, Dias PF, Maraschin M, Ribeiro-do-Valle RM, Lopes-da-Silva JA. Nanofibrous poly(3-hydroxybutyrate-co-3-hydroxyvalerate)/chitosan scaffolds for skin regeneration. *Int J Biol Macromol*. 2012;51:343–50.
- Ma G, Yang D, Wang K, Han J, Ding S, Song G, Nie J. Organic-soluble chitosan/polyhydroxybutyrate ultrafine fibers as skin regeneration prepared by electrospinning. *J Appl Polym Sci*. 2010;118:3619–24.
- Ni Y, Huang Ch, Kokot S. A kinetic spectrophotometric method for the determination of ternary mixtures of reducing sugars with the aid of artificial neural networks and multivariate calibration. *Anal Chim Acta*. 2003;480:53–65.
- Skrbic Z, Divjakovic V. Temperature influence on changes of parameters of the unit cell of biopolymer PHB. *Polymer*. 1996; 37(3):505–07.
- Medvecký L, Giretova M, Stulajterova R. Properties and in vitro characterization of polyhydroxybutyrate–chitosan scaffolds prepared by modified precipitation method. *J Mater Sci Mater Med*. 2014; 25(3):777–89.
- Padermshoke A, Katsumoto Y, Sato H, Ekgasit S, Noda I, Ozaki Y. Melting behavior of poly(3-hydroxybutyrate) investigated by two-dimensional infrared correlation spectroscopy. *Spectrochim Acta Part A*. 2005;61:541–50.
- Ibrahim M, Osman O, Mahmoud AA. Spectroscopic analyses of cellulose and chitosan:FTIR and modeling approach. *J Comput Theor Nanosci*. 2011;8:117–23.
- Kumirska J, Czerwicka M, Kaczyński Z, Bychowska A, Brzozowski K, Thöming J, Stepnowski P. Application of spectroscopic methods for structural analysis of chitin and chitosan. *Mar Drugs*. 2012;8:1567–636. doi:10.3390/md8051567
- Nah JW, Jang MK. Spectroscopic characterization and preparation of low molecular, water-soluble chitosan with free-amine group by novel method. *J Polym Sci Part A*. 2002;40:3796–803.
- Thamaraiselvi TV, Prabakaran K, Rajeswari S. Synthesis of hydroxyapatite thatmimic bone mineralogy. *Trends biomater. Artif Organs*. 2006;19(2):81–3.

29. Slosarczyk A, Paszkiewicz Z, Paluszkiwicz C. FTIR and XRD evaluation of carbonated hydroxyapatite powders synthesized by wet methods. *J Mol Struct*. 2005;744–747:657–61.
30. Tachaboonyakiat W, Netswasdi N, Srakaew V, Opaprakasit M. Elimination of inter- and intramolecular crosslinks of phosphorylated chitosan by sodium salt formation. *Polym J*. 2010;42:148–56.
31. Takagi O, Kuramoto N, Ozawa M, Suzuki S. Adsorption/desorption of acidic and basic proteins on needlelike hydroxyapatite filter prepared by slip casting. *Ceram Int*. 2004;30:139–43.
32. Chou YF, Huang W, Dunn JC, Miller TA, Wu BM. The effect of biomimetic apatite structure on osteoblast viability, proliferation, and gene expression. *Biomaterials*. 2005;26:285–95.
33. Woo KM, Seo J, Zhang R, Ma PX. Suppression of apoptosis by enhanced protein adsorption on polymer / hydroxyapatite composite scaffolds. *Biomaterials*. 2007;28:2622–30.
34. Shi Z, Huang X, Cai Y, Tang R, Yang D. Size effect of hydroxyapatite nanoparticles on proliferation and apoptosis of osteoblast-like cells. *Acta Biomater*. 2009;5:338–45.
35. Kizuki T, Ohgaki M, Katsura M, Nakamura S, Hashimoto S, Toda T, Udagawa S, Yamashita K. Effect of bone-like layer growth from culture medium on adherence of osteoblastlike cells. *Biomaterials*. 2003;24:941–47.
36. Yuasa T, Miyamoto Y, Ishikawa K, Takechi M, Momota Y, Tatehara S, Nagayama M. Effects of apatite cements on proliferation and differentiation of human osteoblasts in vitro. *Biomaterials*. 2004;25:1159–66.
37. Herten M, Rothamel D, Schwarz F, Friesen K, Koegler G, Becker J. Surface- and nonsurface-dependent in vitro effects of bone substitutes on cell viability. *Clin Oral Invest*. 2009;13:149–55.
38. Okada S, Ito H, Nagai A, Komotori J, Imai H. Adhesion of osteoblast-like cells on nanostructured hydroxyapatite. *Acta Biomater*. 2010;6:591–97.
39. Himno S, Tsuchida H, Nagao N. N-acetylation in chitosan and the rate of its enzymatic hydrolysis. *Biomaterials*. 1989;10:574–76.
40. Pangburn SH, Trescony PV, Heller J. Lysozyme degradation of partially deacetylated chitin, its films and hydrogels. *Biomaterials*. 1982;3:105–08.
41. Varum KM, Holme HK, Izume M, Stokke BT, Smidsrod O. Determination of enzymatic hydrolysis specificity of partially N-acetylated chitosans. *Biochim Biophys Acta*. 1996;1291:5–15.
42. Davies RC, Neuberger A, Wilson BM. The dependence of lysozyme activity on pH and ionic strength. *Biochim Biophys Acta*. 1969;178:294–305.
43. Deligianni DD, Katsala ND, Koutsoukos PG, Missirlis YF. Effect of surface roughness of hydroxyapatite on human bone marrow cell adhesion, proliferation, differentiation and detachment strength. *Biomaterials*. 2001;22:87–96.
44. Rizzi SC, Heath DJ, Coombes AGA, Bock N, Textor M, Downes S. Biodegradable polymer/hydroxyapatite composites: Surface analysis and initial attachment of human osteoblasts. *J Biomed Mater Res*. 2001;55:475–86.
45. Sadat-Shojai M, Khorasani MT, Jamshidi A, Irani S. Nano-hydroxyapatite reinforced polyhydroxybutyrate composites: A comprehensive study on the structural and in vitro biological properties. *Mater Sci Eng C*. 2013;33:2776–87.
46. Wu CS, Hsu YC, Liao HT, Cai YX. Antibacterial activity and in vitro evaluation of the biocompatibility of chitosan-based polysaccharide/polyester membranes. *Carbohydr Polym*. 2015;134:438–47.
47. Tanase CE, Sartoris A, Popa MI, Verestiuc L, Unger RE, Kirkpatrick CJ. In vitro evaluation of biomimetic chitosan–calcium phosphate scaffolds with potential application in bone tissue engineering. *Biomed Mater*. 2013;8:025002. doi:[10.1088/1748-6041/8/2/025002](https://doi.org/10.1088/1748-6041/8/2/025002)